NATIONAL ADVISORY COMMITTEE FOR AERONAUTICS

TECHNICAL NOTE 1954

EXPERIMENTAL AND THEORETICAL DISTRIBUTION OF FLOW PRODUCED BY INLET GUIDE VANES OF AN AXIAL-FLOW COMPRESSOR

By Harold B. Finger, Harold J. Schum, and Howard A. Buckner, Jr.

Lewis Flight Propulsion Laboratory
Cleveland, Ohio

NACA

Washington
October 1949

NATIONAL ADVISORY COMMITTEE FOR AERONAUTICS

TECHNICAL NOTE 1954

EXPERIMENTAL AND THEORETICAL DISTRIBUTION OF FLOW PRODUCED

BY INLET GUIDE VANES OF AN AXIAL-FLOW COMPRESSOR

By Harold B. Finger, Harold J. Schum
and Howard A. Buckner, Jr.

SUMMARY

A cascade investigation has been conducted to determine the performance of a set of inlet guide vanes designed for use in a multistage axial-flow compressor and to compare the performance with that predicted by a cylindrical-cascade evaluation method. The method determines the velocities at the outlet of the blade row when the flow-angle and total-enthalpy distributions are known and when the simplified-radial-equilibrium relation is satisfied. The measured flow angles are compared with the angles predicted by an empirical rule. Radial survey data were obtained at the inlet and the outlet of the guide vanes for specific weight flows of 27.95, 31.78, 36.12, and 38.86 pounds per second per square foot outlet-annulus area.

The effect of weight flow on the radial distributions of total pressure and flow angle was small. The deviation angle was substantially constant over the central portion of the passage but increased toward the tip. For camber angles above 30°, a critical Mach number at which the lift coefficient decreases with increasing Mach number was obtained at a specific weight flow of 38.86 pounds per second per square foot. When the radial distribution of flow angle was known, the guide-vane outlet velocities over the central portion of the passage could be computed by a cylindrical-cascade evaluation method within an accuracy of 2 percent.

INTRODUCTION

The purpose of inlet guide vanes for axial-flow compressors is to deliver the air efficiently to the first row of rotor blades at the desired angles of attack. Although the design of inlet guide vanes should be a relatively simple task in view of the low angles of incidence, the small amount of turning usually required, and the favorable pressure gradient through the blade row, prediction

of performance has been difficult. On the basis of a two-dimensional
cascade investigation, design charts that can be used to design
inlet guide vanes having specific NACA airfoil sections are pre-
sented in reference 1. If no experimental data are available, the
designer must use some empirical rule or a potential-flow theory as
a basis for the design of guide vanes and the blades are altered as
necessitated by experiment.

    An investigation was conducted at the NACA Lewis laboratory to
provide experimental data on inlet guide vanes where the flow veloc-
ities are relatively high and where three-dimensional effects are
appreciable. These data are compared to the results predicted by
a cylindrical-cascade evaluation method by which the outlet veloc-
ities may be determined when the flow-angle and total-enthalpy dis-
tributions are known. The method is applicable to any blade row
when simplified radial equilibrium exists. A comparison between
the measured flow angles and the angles predicted by a rule that
is a revision of Constant's rule (reference 2) and considers the
effect of blade stagger on flow angle is also made.

ANALYSIS

    The design of an axial-flow-machine blade row requires a knowl-
edge of total-enthalpy, flow-angle, and velocity distributions at
the outlet of the preceding blade row. A relation is therefore
necessary that can be used to solve for any one of the variables
when the others are specified. Because the total enthalpy and the
flow angles can be readily measured in an experimental investiga-
tion and can be specified in a design procedure, a relation express-
ing the axial and tangential velocities as functions of enthalpy
and flow angle at any given mass flow would facilitate design pro-
cedures and the determination of cascade performance.

    The following discussion presents the development of such a
cylindrical-cascade evaluation method. All symbols are defined
in appendix A.

    The energy equation for compressible flow can be stated as

$$t = T - \frac{1}{2} \frac{V_\theta^2}{c_p Jg} - \frac{1}{2} \frac{V_z^2}{c_p Jg} - \frac{1}{2} \frac{V_r^2}{c_p Jg} \tag{1}$$

Differentiation of equation (1) with respect to the radius gives

$$\frac{dt}{dr} = \frac{dT}{dr} - \frac{1}{2c_p Jg}\frac{d(V_\theta^2)}{dr} - \frac{1}{2c_p Jg}\frac{d(V_z^2)}{dr} - \frac{1}{2c_p Jg}\frac{d(V_r^2)}{dr} \qquad (2)$$

The fundamental relation between total- and static-gas condi-
tions at a point is given by

$$\frac{P_1^{\frac{\gamma-1}{\gamma}}}{T_1} = \frac{p_1^{\frac{\gamma-1}{\gamma}}}{t_1} = K$$

or

$$\frac{\gamma-1}{\gamma}\log_e P_1 - \log_e T_1 = \frac{\gamma-1}{\gamma}\log_e p_1 - \log_e t_1 = 0$$

Differentiation with respect to the radius and transposition
of terms gives

$$\frac{dt_1}{dr} = \frac{\gamma-1}{\gamma}\frac{t_1}{p_1}\frac{dp_1}{dr} = \frac{1}{c_p\,\rho_1}\frac{dp_1}{dr} \qquad (3)$$

Equation (3) requires that the losses be constant along the radius.

If the relation of equation (3) is substituted into equation (2)

$$\left[\frac{dT}{dr} - \frac{1}{2c_p Jg}\frac{d(V_\theta^2)}{dr} - \frac{1}{2c_p Jg}\frac{d(V_z^2)}{dr} - \frac{1}{2c_p Jg}\frac{d(V_r^2)}{dr}\right] = \frac{1}{c_p\,\rho_1}\frac{dp_1}{dr}$$

$$(4)$$

For radial equilibrium, if the assumption is made that $\dfrac{\partial V_r}{\partial r}$
or V_r and $\dfrac{\partial V_r}{\partial z} = 0$,

$$\frac{1}{\rho}\frac{dp}{dr} = \frac{V_\theta^2}{r} \qquad (5)$$

When $V_r = 0$, equations (4) and (5) combine to yield

$$\frac{dT}{dr} - \frac{1}{2c_p Jg} \frac{d(V_\theta{}^2)}{dr} - \frac{1}{2c_p Jg} \frac{d(V_z{}^2)}{dr} - \frac{1}{c_p Jg} \frac{V_\theta{}^2}{r} = 0 \qquad (6)$$

Equation (6) expresses the relation between the gas veloci-
ties and the gas state where radial velocities are negligible and
when the losses are constant along the radius.

From the vector-diagram geometry

$$V_\theta = V_z \tan \alpha$$

and

$$\frac{d(V_\theta{}^2)}{dr} = 2V_z{}^2 \sec^2 \alpha \tan \alpha \frac{d\alpha}{dr} + \tan^2 \alpha \frac{d(V_z{}^2)}{dr}$$

Substitution of the geometrical relations into equation (6)
gives

$$c_p Jg \frac{dT_1}{dr} = \frac{V_z{}^2}{r}\left(\tan^2 \alpha + r \tan \alpha \sec^2 \alpha \frac{d\alpha}{dr}\right) + \frac{1}{2} \frac{d(V_z{}^2)}{dr} \sec^2 \alpha$$

Division of the preceding equation by $\frac{1}{2} \sec^2 \alpha$ gives

$$c_p Jg \frac{dT_1}{dr} \frac{1}{\sec^2 \alpha} = 2V_z{}^2 \left(\frac{\sin^2 \alpha}{r} + \tan \alpha \frac{d\alpha}{dr}\right) + \frac{d(V_z{}^2)}{dr} \qquad (7)$$

Let

$$2\left(\frac{\sin^2 \alpha}{r} + \tan \alpha \frac{d\alpha}{dr}\right) = S$$

and

$$\frac{2}{\rho_o} \frac{dP}{dr} \frac{1}{\sec^2 \alpha} = Q$$

Therefore, at any radius, equation (7) will be

$$SV_z{}^2 + \frac{d(V_z{}^2)}{dr} = Q$$

or

$$SV_z{}^2dr + d(V_z{}^2) = Qdr$$

which is a first-order differential equation linear in $V_z{}^2$ that has the following solution:

$$\left[V_z{}^2 \exp\left(\int_{r_h}^r S\ dr\right)\right]_{r_h}^r = \int_{r_h}^r Q \exp\left(\int_{r_h}^r S\ dr\right) dr$$

If the values of S and Q are substituted

$$\left\{V_z{}^2 \exp\left[\int_{r_h}^r \left(\frac{2\ \sin^2 \alpha}{r} + 2\ \tan \alpha\ \frac{d\alpha}{dr}\right) dr\right]\right\}_{r_h}^r$$

$$= \int_{T_h}^T \frac{2c_p Jg\ dT}{\sec^2 \alpha} \exp\left[\int_{r_h}^r \left(\frac{2\ \sin^2 \alpha}{r} + 2\ \tan \alpha\ \frac{d\alpha}{dr}\right) dr\right]$$

$$(8)$$

The exponential in equation (8) can be integrated as follows:

$$\int_{r_h}^r \left(\frac{2\ \sin^2 \alpha}{r} + 2\ \tan \alpha\ \frac{d\alpha}{dr}\right) dr = \int_{r_h}^r 2\ \sin^2 \alpha\ \frac{dr}{r} - \left[2\ \log_e\ \cos \alpha\right]_{\alpha_h}^{\alpha}$$

$$= \int_{r_h}^r 2\ \sin^2 \alpha\ \frac{dr}{r} + 2\ \log_e\left(\frac{\cos \alpha_h}{\cos \alpha}\right)$$

Therefore

$$\exp\left[\int\left(\frac{2\sin^2\alpha}{r}+2\tan\alpha\frac{d\alpha}{dr}\right)dr\right]=\left(\frac{\cos\alpha_h}{\cos\alpha}\right)^2\exp\left(\int_{r_h}^{r}2\sin^2\alpha\frac{dr}{r}\right)$$

$$(9)$$

By application of equation (9), equation (8) reduces to

$$\left[V_z^2\left(\frac{\cos\alpha_h}{\cos\alpha}\right)^2\exp\left(\int_{r_h}^{r}2\sin^2\alpha\frac{dr}{r}\right)\right]_{r_h}^{r}$$

$$=\int_{T_h}^{T}2c_pJg\cos^2\alpha_h\exp\left(\int_{r_h}^{r}2\sin^2\alpha\frac{dr}{r}\right)dT$$

This equation can be further reduced to

$$V_z^2\left(\frac{\cos\alpha_h}{\cos\alpha}\right)^2\exp\left(\int_{r_h}^{r}2\sin^2\alpha\frac{dr}{r}\right)-V_{z,h}^2$$

$$=\int_{T_h}^{T}2c_pJg\cos^2\alpha_h\exp\left(\int_{r_h}^{r}2\sin^2\alpha\frac{dr}{r}\right)dT\qquad(10)$$

From the continuity equation

$$W=\int_{r_h}^{r_t}2\pi r\,dr\,\rho g V_z=\int_{r_h^2}^{r_t^2}\pi\rho g V_z\,d(r^2)\qquad(11)$$

As a first approximation, ρ will be assumed constant along the radius and equal to a value indicated by a wall static-pressure measurement in order to reduce the number of trials necessary.

Equations (10) and (11) can be simultaneously solved by a trial-and-error method. An assumed value of $V_{z,h}$ is substituted in equation (10) so that V_z can be determined as a function of the radius. The term $\displaystyle\int_{r_h^2}^{r_t^2} \pi\rho g V_z \, d(r^2)$ can then be calculated and its value checked by the continuity relation given in equation (11). This procedure is repeated until the values of the integrals determined by the two methods check.

A new radial distribution of density can be determined by combining the energy equation and isentropic relation to give

$$\frac{\rho}{\rho_o} = \left[1 - \frac{(\gamma-1)}{2} \frac{V^2}{\gamma gRT}\right]^{\frac{1}{\gamma-1}}$$

or

$$\frac{\rho}{\rho_o} = \left[1 - \frac{(\gamma-1)}{2} \frac{V_z^2}{\gamma gRT \cos^2 \alpha}\right]^{\frac{1}{\gamma-1}} \tag{12}$$

The distribution of density determined from equation (12) is then substituted in equation (11) and the procedure is repeated until the final density distribution checks the one used in the continuity equation. The velocity distribution can be determined from the known distributions of total enthalpy and outlet angle.

The preceding solution can be used to determine the flow from any blade row, rotor, or stator (if the simplified-radial-equilibrium relation is satisfied). In a design procedure, the conditions upstream of the rotor are usually prescribed. Then, by specifying the distribution of work in the rotor the distribution of total enthalpy downstream of the rotor is determined. The radial distribution of absolute flow angle is generally specified by the type of flow desired so that the method of determining the velocity distributions can be used as part of a design procedure. Corrections could be made for boundary layers at the annulus walls by assuming the distribution of total enthalpy in the boundary layer and substituting in equation (10), or more simply by applying a correction factor in the continuity relation.

If the total temperature is practically constant along the radius, as was the case in the present investigation, equation (10) becomes

$$V_z^2 \frac{\cos \alpha_h}{\cos \alpha} \exp\left(\int_{r_h}^{r} 2 \sin^2 \alpha \frac{dr}{r}\right) - V_{z,h}^2 = 0$$

and

$$\frac{V_z}{V_{z,h}} = \frac{\cos \alpha}{\cos \alpha_h} \exp\left(\int_{r}^{r_h} \sin^2 \alpha \frac{dr}{r}\right) \tag{13}$$

The axial velocity at the hub can be determined from the continuity relation

$$V_{z,h} = \frac{W}{2\pi g \int_{r_h}^{r_t} \rho \frac{V_z}{V_{z,h}} r \, dr} \tag{14}$$

The density distribution is determined by the trial-and-error method previously discussed in the general solution of the equations. In this investigation, it was found that the radial variation of density could be neglected.

Because the flow angle from the guide vanes is practically constant over a large range of inlet Mach numbers or weight flows, the exponential in equation (13) and the resulting ratio of axial velocities need be evaluated only once.

The radial distribution of axial velocity was determined in the present investigation by combining equations (13) and (14) and solving graphically.

APPARATUS AND PROCEDURE

Inlet guide vanes. - The inlet guide vanes used in the investigation were designed for an axial-flow compressor with a specific weight flow at the first row of rotor blades of approximately 40 pounds of air per second per square foot of annulus area at

sea-level inlet-air conditions. The blades of the guide-vane cas-
cade are shrouded at both the tip and the root. These shrouds are
tapered to form an annular flow area that converges between the
inlet and the outlet of the cascade. The outlet tip-to-hub radius
ratio of the guide vanes is 2.0. The solidity of the guide vanes
varies from 1.75 at a radius ratio of 1.0 to 1.0 at a radius ratio
of 1.8.

   The airfoil sections have a parabolic-arc camber line. The
trailing edges of the blades are on a radial line. The blade-
camber angle varies from approximately 25° at the root to 35° at
the tip and the stagger angle (angle between chord and axial
direction) varies from approximately 12° to 20°. The maximum
thickness is of the order of 6 percent of the chord length and
occurs at approximately 35 percent of the chord. The maximum
camber occurs at approximately 40 percent of the chord.

   Setup. - A diagrammatic drawing of the setup used in the inves-
tigation of the flow through the guide vanes is shown in figure 1.
The guide-vane cascade was mounted in a cast-aluminum inlet section
(fig. 1). A hemispherical hub was attached to the entrance of the
inlet section. The straight annular air passage in the inlet sec-
tion faired smoothly into the guide-vane cascade. The inlet sec-
tion had four airfoil-shaped struts that would normally support
the compressor front-bearing housing and accessory drive.

   Ambient air entered the unit through a thin-plate orifice
mounted on the intake end of an orifice tank, 3 feet in diameter
and 12 feet in length. A $13\frac{1}{2}°$ conical reducer, $17\frac{1}{2}$ inches in
length, was fitted between the orifice tank and the inlet section
to provide a favorable pressure gradient in the direction of flow.
The inlet section with the guide vanes in position was bolted to a
discharge adapting section made annular by a wood inner cylinder.
The inner and outer diameters of this annular discharge passage
simulated those of the hub and the casing of the first stage in
the axial-flow compressor. The length of the annular discharge
passage was $14\frac{1}{2}$ inches. The air was discharged through an elbow
into the laboratory altitude exhaust system. A 1/2-inch-mesh
75-percent opening screen was located immediately upstream of the
elbow to reduce circumferential variations.

   Instrumentation. - The setup was instrumented to determine
the following quantities: gas state upstream of the flow-
measuring orifice, static-pressure drop across the orifice, gas
state at the inlet measuring station upstream of the blade row,
radial variation in velocity at the inlet measuring station,
circumferential distribution of static pressure on the inner

and outer walls at inlet and outlet measuring stations, gas state
at outlet measuring station, and the radial variations of velocity
and flow angle at the outlet measuring station.

The inlet-air temperature was measured with a liquid-in-glass
thermometer. A wall static tap located according to reference 4
was used to measure the orifice pressure drop, which was indicated
on a water manometer.

The inlet measuring station was located in the straight annular
portion of the compressor-inlet section, approximately $1\frac{1}{2}$ chord
lengths upstream of the leading edge of the guide vanes, as shown
in figure 1. Four wall static-pressure taps were located at this
station between struts on both the inner and outer walls, $22\frac{1}{2}^{\circ}$
apart; the taps on the outer wall were located on the same radial
elements as those of the inner wall. A hook-type static-pressure
probe (fig. 2(a)) and a shielded total-pressure probe (fig. 2(b))
insensitive to yaw to approximately $\pm45^{\circ}$ were located at this sta-
tion to measure the radial pressure distribution.

The outlet measuring station was located in a plane approxi-
mately 2 chord lengths downstream of the trailing edge of the guide
vanes (fig. 1). Four wall static-pressure taps were located at
this station on both the inner and outer walls and in the same
axial planes as those of the inlet station. A static-pressure
probe of the type used at the inlet was also located at this sta-
tion. In addition, a two-hole Fechheimer tube (fig. 2(c)) was
used to measure the radial distribution of flow angle and total
pressure.

Instrumentation was located to avoid measurement in the wakes
of the airfoil sections. Inlet pressures were indicated on a
common-well water manometer board; outlet pressures were indicated
on mercury manometers.

Procedure. - Survey runs were made at values of specific
weight flow of 27.95, 31.78, 36.12, and 38.86 pounds per second
per square foot annulus area, which are in the high weight-flow
range for these guide vanes. Air flow was regulated by a butter-
fly throttle valve in the exhaust line. The weight flow was main-
tained constant to within ±0.5 percent while the various measure-
ments were made. The Reynolds numbers, based on the outlet
conditions encountered in the present investigation with the blade
chord as the characteristic dimension, were in the range of 300,000
to 500,000. The effects of variation of Reynolds number in this
range were assumed to be small.

Precision. - The accuracy with which all measurements were made is estimated to be within the following limits:

Inlet pressure, inches of water . . . . ±0.05
Outlet pressure, inches of mercury . . . . ±0.05
Flow angle, degrees . . . . ±1.0
Weight flow, percent . . . . ±0.5
Velocity, percent . . . . ±0.5

Calibration of the static-pressure probe showed that the maximum error of the instrument up to an indicated Mach number of about 0.75 was 2 percent of the indicated velocity pressure. The shielded total-pressure probe used at the inlet station was found to be insensitive to yaw to approximately ±45°.

A further error was induced by assuming that radial surveys at corresponding points between adjacent blades were sufficient for specifying the cascade performance. Because no circumferential surveys were made, the data could not be corrected for circumferential variations. An indication of the effect of circumferential position was obtained from measurements of wall static pressure that gave variations around the inner and outer walls of as much as 12 percent of the velocity pressure, which resulted in a maximum variation in velocity of approximately ±2 percent. These random circumferential variations were caused by inaccuracies in setting the vanes in position. Measurements indicated that the blade-angle settings varied as much as $3°$ or $3\frac{1}{2}°$. It is believed that the blade spacing also varied appreciably. Additional variations may have been introduced by the elbow behind the test section.

Calculations. - The weight of air flowing through the guide vanes was computed from the orifice data by the method recommended in reference 3. This weight-flow determination was checked by integrating the velocity profiles at the inlet and the outlet of the guide vanes. In general, the inlet-station measurements checked the orifice measurement within 2 percent and the corresponding agreement with the measurements at the outlet station was within 3 percent.

Values of absolute velocity were calculated from the static- and total-pressure measurements by using the relation

$$V = \sqrt{\frac{2\gamma gRT}{\gamma-1} \left[1 - \left(\frac{p}{P}\right)^{\frac{\gamma-1}{\gamma}} \right]}$$

based on the Bernoulli equation and the isentropic gas laws. Axial
and tangential velocities were computed from the resultant velocity
and the measured flow angle.

The following expression, which is derived in appendix B, was
used to determine lift coefficients for the guide vanes:

$$C_L = \frac{8\,\frac{s}{c}\,\frac{V_2}{V_1}\,\sin\alpha_2}{\left(1 + \frac{V_2}{V_1}\cos\alpha_2\right)\sqrt{\left(1 + \frac{V_2}{V_1}\cos\alpha_2\right)^2 + \left(\frac{V_2}{V_1}\sin\alpha_2\right)^2}}$$

This equation assumed that the lift force is perpendicular to the
vectorial mean of the inlet and outlet velocities. This assumed
lift differs slightly from the theoretical force resulting from
momentum and pressure considerations.

RESULTS AND DISCUSSION

Guide-Vane Performance

The results of the investigation are presented as radial dis-
tributions of pressures, angles, velocities, and lift coefficients.

Inlet survey data. - The results of the surveys at the inlet
measuring station for the specific weight flows investigated are
presented in figures 3 to 5. Curves of inlet total and inlet
static pressure divided by atmospheric pressure are shown in fig-
ures 3 and 4, respectively, as functions of the ratio of the
radius at any point in the flow passage to the hub radius. Fig-
ure 5 presents the velocity of the air at the inlet measuring
station plotted against the radius ratio.

The inlet total pressure was fairly constant over most of
the flow passage, decreasing slightly as the air weight flow was
increased. At the tip, however, there was a marked decrease in
total pressure, probably resulting from viscous effects at the
duct wall upstream of the measuring station. In any case, the
nonuniform inlet-total-pressure distribution did not appreciably
affect the results at the outlet because calculations have indi-
cated that the maximum change in resultant outlet velocity due
to the nonuniform profile was less than 5 percent.

The radial distribution of inlet static pressure (fig. 4) is of the form that might be expected from flow upstream of a convergent channel; that is, the static pressure at the center of the passage is less than that at either wall.

The radial distribution of velocity at the inlet measuring station is presented in figure 5 for the four weight flows investigated. The inlet velocities were found to have no tangential components. The decrease in inlet velocity near the outer wall follows the same form as that of the inlet-total pressure distribution. The velocities immediately upstream of the guide vanes can be computed from the data taken at the inlet measuring station by application of the continuity equation, if incompressible flow and zero incidence are assumed.

Outlet survey data. - The results of the radial surveys at the outlet measuring station are presented in figures 6 to 9 as the ratios of outlet total and static pressure to atmospheric pressure, outlet deviation angle, and outlet velocity plotted against radius ratio. The ratio of outlet total pressure to atmospheric pressure (fig. 6) was approximately constant over the central portion of the annular passage area but dropped in the boundary layer near the tip. A similar situation probably occurred at the inner wall; no data were taken close to the hub, however, because of the configuration of the yaw tube. The total pressure decreased slightly as the weight flow was increased, indicating increased losses.

The static pressure at the outlet measuring station increased uniformly from the hub to the tip of the blades (fig. 7). The slope of the static-pressure variation increased slightly as the flow was increased from 27.95 to 38.86 pounds per second per square foot. As shown in figure 7, the static-pressure gradient at the measuring station (2 chord lengths downstream of the cascade) was practically that gradient which is required for the simplified-radial-equilibrium condition where the radial velocity and the axial variation of radial velocity is negligible. Immediately downstream of the guide vanes, the distribution of static pressure would differ from that at the measuring station because of the radial flow induced by the convergent inner and outer shrouds. For axially symmetric flow, the condition of radial equilibrium of forces immediately behind the guide vane is

$$\frac{1}{\rho} \frac{dp}{dr} = \frac{V_\theta^2}{r} - V_z \frac{\partial Vr}{\partial z} - Vr \frac{\partial Vr}{\partial r}$$

The simplified-radial-equilibrium relation, which was found to
exist at the outlet measuring station, assumed that the last two
terms in the preceding equation are negligible.

The radial distribution of air-outlet deviation angle (angle
between trailing-edge camber line and outlet-air velocity) is pre-
sented in figure 8 for the four weight flows investigated. The
deviation angle decreased slightly from a radius ratio of 1.1 to
a radius ratio of approximately 1.45. At this point, the devia-
tion angle increased slightly until the boundary layer was reached
through which the deviation decreased sharply because of the
decrease in axial velocity. If the precision of measurement is
considered, however, the deviation is practically constant at 2^O
over the central portion of the passage. For these vanes, the
effect of the increasing camber angle from hub to tip is inversely
proportional to the effect of the decreasing solidity so that the
two factors counterbalance each other and cause the deviation to
remain substantially constant. No flow-angle measurements were
taken close to the hub because of the Fechheimer instrument
geometry, which was such as to prevent tube-end effects on the
measurements. The effect of weight flow on the angle distribu-
tion was practically negligible giving a maximum over-all varia-
tion of 2^O. Immediately behind the guide vanes, the effects of
the finite blade and wake thicknesses and the boundary layer may
give a different flow-angle distribution than that existing at
the outlet measuring station.

The radial variations in resultant, axial, and tangential
velocities at the outlet measuring station are presented in fig-
ure 9 for the air weight flows considered.

The trends of the corresponding velocity distributions are
the same for all the flow conditions; the axial and resultant
velocities decrease and the tangential component increases with
radius ratio. These trends are caused by the effects of solidity
on axial velocity and of camber angle on tangential velocity.

Lift coefficient. - The distribution of lift coefficient as
computed from the equation developed in appendix B is presented
in figure 10 for the four air weight flows investigated as a
function of camber angle and solidity. For camber angles below
30° and solidities above 1.2, the effect of weight flow or Mach
number on lift coefficient is practically negligible. At higher
camber angles, however, the lift coefficient for a specific
weight flow of 38.86 pounds per second per square foot is slightly
lower than those for specific weight flows of 36.12, 31.78, and
27.95 pounds per second per square foot. The low lift coefficient

at the highest specific weight flow seems to be caused by the
attainment of a critical Mach number at which the lift decreases
with increase in Mach number. The small effects of Mach number on
velocity ratio (resulting from total-pressure loss) and turning
angle apparently combine to cause a noticeable effect on lift
coefficient.

<div align="center">Comparison of Experimental Results with

Analytical Results</div>

The problem of designing accelerating inlet guide vanes is
principally one of designing blades that will give a desired flow
distribution into the first row of rotor blades. No simple satis-
factory method has been devised for the design of guide vanes hav-
ing any general profile. Experimental investigations such as that
of reference 1 have resulted in design procedures that are appli-
cable to the specific airfoils investigated.

Turning angle. - One of the difficulties in inlet-guide-vane
design is that of setting the blades to give desired outlet flow
angles. The method of redesigning after testing is costly and
time-consuming. Empirical design rules based on various theo-
retical and experimental investigations are most satisfactory
because of the ease with which they can be applied. A rule,
which is based on potential-flow considerations and is a more
exact form of Constant's rule (reference 2), is therefore used
herein to determine the deviation angles. Because the blade pro-
file used in this investigation was very similar to the parabolic-
arc-cambered airfoil investigated in reference 2, the rule was
assumed applicable without further revision by the potential-flow
methods. The constant in the rule is a function of the blade
stagger angle, which is defined as the angle between the chord and
the axial direction. Comparison of the deviation angles predicted
by the empirical rule with the measured angles is presented in
figure 11 for a specific weight flow of 36.12 pounds per second
per square foot. Near the hub, the measured and computed results
agree within the precision of measurement. The maximum differ-
ence between the measured and computed angles is approximately 3°
at a radius ratio of 1.65. The difference then decreases toward
the tip and increases in the boundary layer. It must be noted
that the derivation of the empirical rule depends on the camber
and the stagger of the airfoils in cascade and must be altered
by potential-flow methods for each cascade if it is to be made
generally applicable.

Velocity. - Outlet velocities can be predicted over the central portion of flow from the cylindrical-cascade evaluation method based on the energy and continuity relations. The application of this equation assumes that the simplified-radial-equilibrium relation is satisfied and that the radial distribution of flow angle is known.

A comparison of the measured and computed axial velocities is presented in figure 12 for a specific weight flow of 36.12 pounds per second per square foot. The analysis was applied to the measured-angle distribution. Over the central portion of the passage, the predicted axial velocities are a maximum of 2 percent lower than the actual velocities but near the outer wall where the total pressure decreases rapidly the agreement is poor. A similar situation probably exists at the inner wall. The error incurred near the midsection is caused by neglecting the boundary-layer effects, which tend to reduce the effective flow area and thereby give higher actual velocities than predicted ones. The problem of designing accelerating guide vanes with constant total pressure and negligible radial flows therefore reduces to that of predicting turning angles. For such guide vanes, the velocities can be accurately determined if the angles are known. The radial velocities must be considered in the radial-equilibrium expression previously discussed if it is applied to a station immediately downstream of the cascade.

SUMMARY OF RESULTS

The results of this investigation of the performance of the inlet guide vanes from a multistage axial-flow compressor can be summarized as follows:

1. The effect of weight flow on the radial distributions of total pressure and flow angle was small. Deviation angle was practically constant over the central portion of the passage but increased near the tip and then decreased rapidly in the boundary layer at the blade tip. The slope of the variation of static pressure with radius increased with increasing weight flow.

2. For camber angles above $30°$, a critical Mach number at which the lift coefficient decreases with increasing Mach number was attained at a specific weight flow of 38.86 pounds per second per square foot.

3. If the radial distribution of flow angle is known and if the total pressure is constant, the guide-vane outlet velocities over the central portion of the passage can be computed from the cylindrical-cascade evaluation method within an accuracy of 2 percent.

4. The deviation angles predicted by an empirical rule based on Constant's work were approximately 3° higher than the measured angles. The constant in the rule should be altered by potential-flow methods to make the results applicable for any specific blade profile having a parabolic camber line.

Lewis Flight Propulsion Laboratory,
    National Advisory Committee for Aeronautics,
        Cleveland, Ohio, July 14, 1948.

APPENDIX A

SYMBOLS

The following symbols were used in the calculations:

A   annulus area, sq ft

C_L lift coefficient

c   blade chord, ft

c_p specific heat at constant pressure, Btu/(lb)($^\circ$R)

c_v specific heat at constant volume, Btu/(lb)($^\circ$R)

D   blade profile drag, lb/ft, (fig. 13)

exp   base of Napierian logarithmic system raised to power in parentheses following exp

F   resultant force on blade element, lb/ft, (fig. 13)

g   acceleration due to gravity, 32.174 ft/sec^2

J   mechanical equivalent of heat, 778 ft-lb/Btu

L   blade profile lift, lb/ft, (fig. 13)

P   total pressure, lb/sq ft absolute

p   static pressure, lb/sq ft absolute

R   gas constant, 53.5 ft-lb/(lb)($^\circ$R)

r   radius, ft

s   blade spacing, ft

T   total temperature, $^\circ$R

t   static temperature, $^\circ$R

V   air velocity, ft/sec, (fig. 13)

W   weight flow, lb/sec

$\dfrac{W\sqrt{\theta}}{\delta\,A_2}$ specific weight flow, lb/(sec)(sq ft)

z axial distance

α angle between axial direction and air velocity, deg, (fig. 13)

β blade camber angle, (angle between axial direction and tangent to trailing-edge camber line), deg, (fig. 13)

γ ratio of specific heats, c_p/c_v

Δ deviation angle, $\beta - \alpha_2$, deg, (fig. 13)

δ ratio of atmospheric pressure to standard sea-level pressure, 29.92 in. Hg absolute

θ ratio of atmospheric temperature to standard sea-level temperature, 518.4° R

ρ static density, slugs/cu ft

ρ_o total density, slugs/cu ft

σ solidity, c/s

Subscripts:

0   atmospheric conditions

1   inlet measuring station

2   outlet measuring station

h   hub

i   immediately upstream of guide vanes

m   mean

r   radial

t   tip

z   axial

θ tangential

APPENDIX B

DERIVATION OF LIFT COEFFICIENT

For the purpose of this investigation an expression for lift coefficient as a function of turning angle, solidity, and inlet and outlet velocities was desirable. The derivation of this expression is given in the following paragraphs.

By reference to figure 13, the lift force on the blade is

$$L = \frac{F_\theta}{\cos \alpha_m} + D \tan \alpha_m$$

For low-camber blades with fairly small losses, $D \tan \alpha_m$ is sufficiently small to be neglected with little error. Consequently,

$$L = \frac{F_\theta}{\cos \alpha_m} \tag{B1}$$

The component of the resultant force in the direction perpendicular to axial is given by

$$F_\theta = W \left(V_{\theta,2} - V_{\theta,1}\right) \tag{B2}$$

When two-dimensional incompressible flow is assumed, the weight flow per passage and per unit blade length is

$$W = \rho_1 g V_1 s \tag{B3}$$

Because the flow at the inlet is considered to be axial $V_{\theta,1} = 0$ and $V_{\theta,2} = V_2 \sin \alpha_2$, equations (B2) and (B3) may be combined to obtain

$$F_\theta = \rho_1 g V_1^2 s \frac{V_2}{V_1} \sin \alpha_2$$

By substitution in equation (B1),

$$L = \frac{\rho_1 g V_1^2 s \frac{V_2}{V_1} \sin \alpha_2}{\cos \alpha_m}$$

Then

$$C_L = \frac{L}{\frac{1}{2} \rho_1 g V_m^2 c} = \frac{\rho_1 V_1^2 s \frac{V_2}{V_1} \sin \alpha_2}{\frac{1}{2} \rho_1 V_m^2 c \cos \alpha_m}$$

From the diagram,

$$V_m = \frac{V_1 + V_2 \cos \alpha_2}{2 \cos \alpha_m} = \frac{V_1}{2 \cos \alpha_m} \left(1 + \frac{V_2}{V_1} \cos \alpha_2\right)$$

Therefore

$$C_L = \frac{8 \frac{s}{c} \frac{V_2}{V_1} \sin \alpha_2 \cos \alpha_m}{\left(1 + \frac{V_2}{V_1} \cos \alpha_2\right)^2} \qquad (B4)$$

Also, from the diagram

$$\cos \alpha_m = \frac{V_1 + V_2 \cos \alpha_2}{2 \sqrt{\frac{(V_1 + V_2 \cos \alpha_2)^2}{4} + \frac{(V_2 \sin \alpha_2)^2}{4}}}$$

$$= \frac{1 + \left(\frac{V_2}{V_1}\right) \cos \alpha_2}{\sqrt{\left(\frac{V_2}{V_1}\right)^2 + 2\left(\frac{V_2}{V_1}\right) \cos \alpha_2 + 1}}$$

By substitution in equation (B4),

$$C_L = \frac{8 \frac{s}{c} \frac{V_2}{V_1} \sin \alpha_2}{\left(1 + \frac{V_2}{V_1} \cos \alpha_2\right) \sqrt{\left(1 + \frac{V_2}{V_1} \cos \alpha_2\right)^2 + \left(\frac{V_2}{V_1} \sin \alpha_2\right)^2}}$$

REFERENCES

1. Zimmey, Charles M., and Lappi, Viola M.: Data for Design of
      Entrance Vanes from Two-Dimensional Tests of Airfoils in
      Cascade. NACA ACR L5G18, 1945.

2. Constant, H.: Note on Performance of Cascades of Aerofoils.
      Rep. No. E. 3696, R.A.E., June 1939.

3. Ebaugh, N. C., and Whitfield, R.: The Intake Orifice and a Pro-
      posed Method for Testing Exhaust Fans. A.S.M.E. Trans.,
      PTC-56-3, vol. 56, no. 12, Dec. 1934, pp. 903-911.
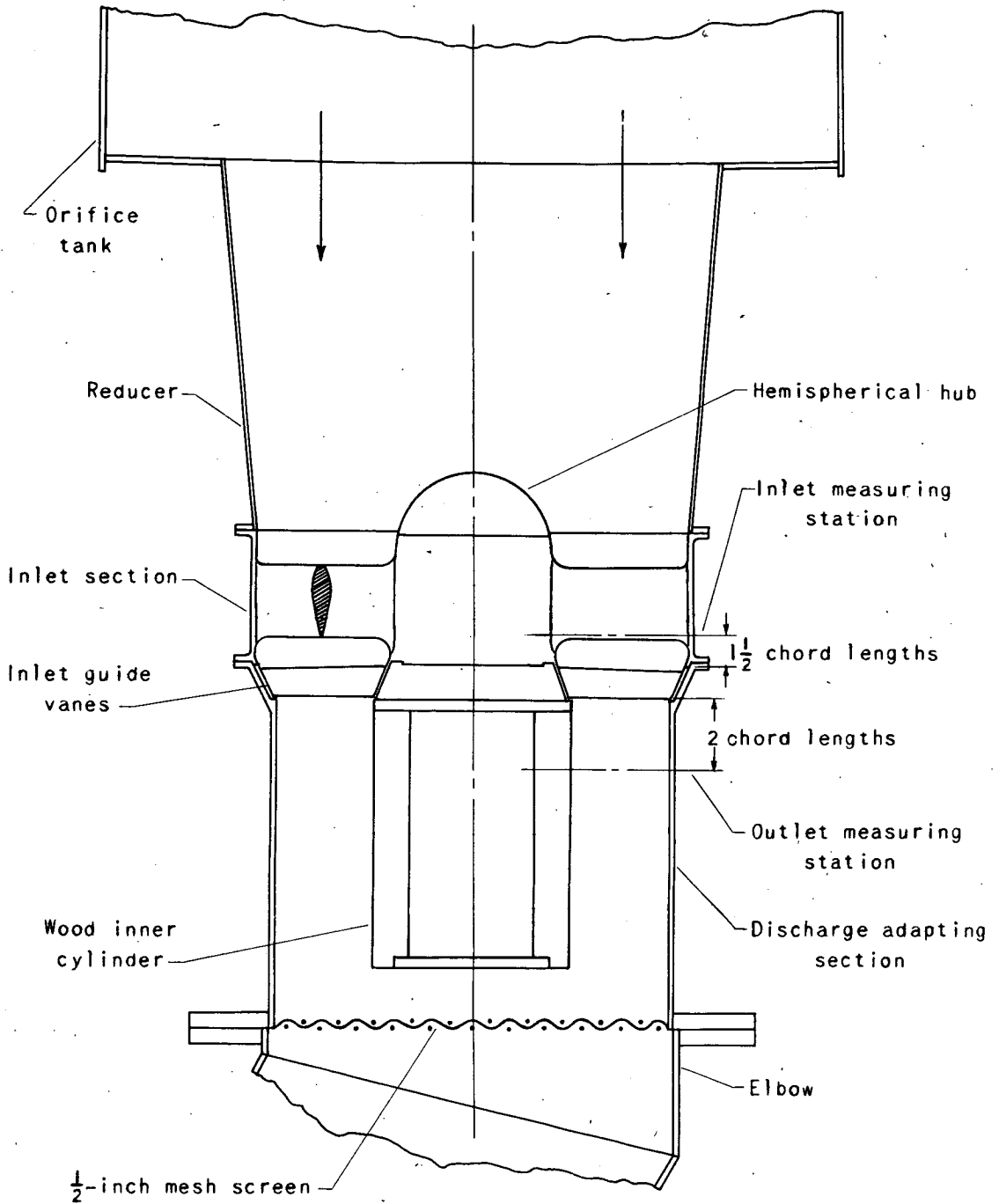
Figure 1. - Schematic drawing of setup.

Page intentionally left blank

Page intentionally left blank

(a) Static-pressure probe.   (b) Shielded total-pressure probe.   (c) Two-hole Fechheimer tube.
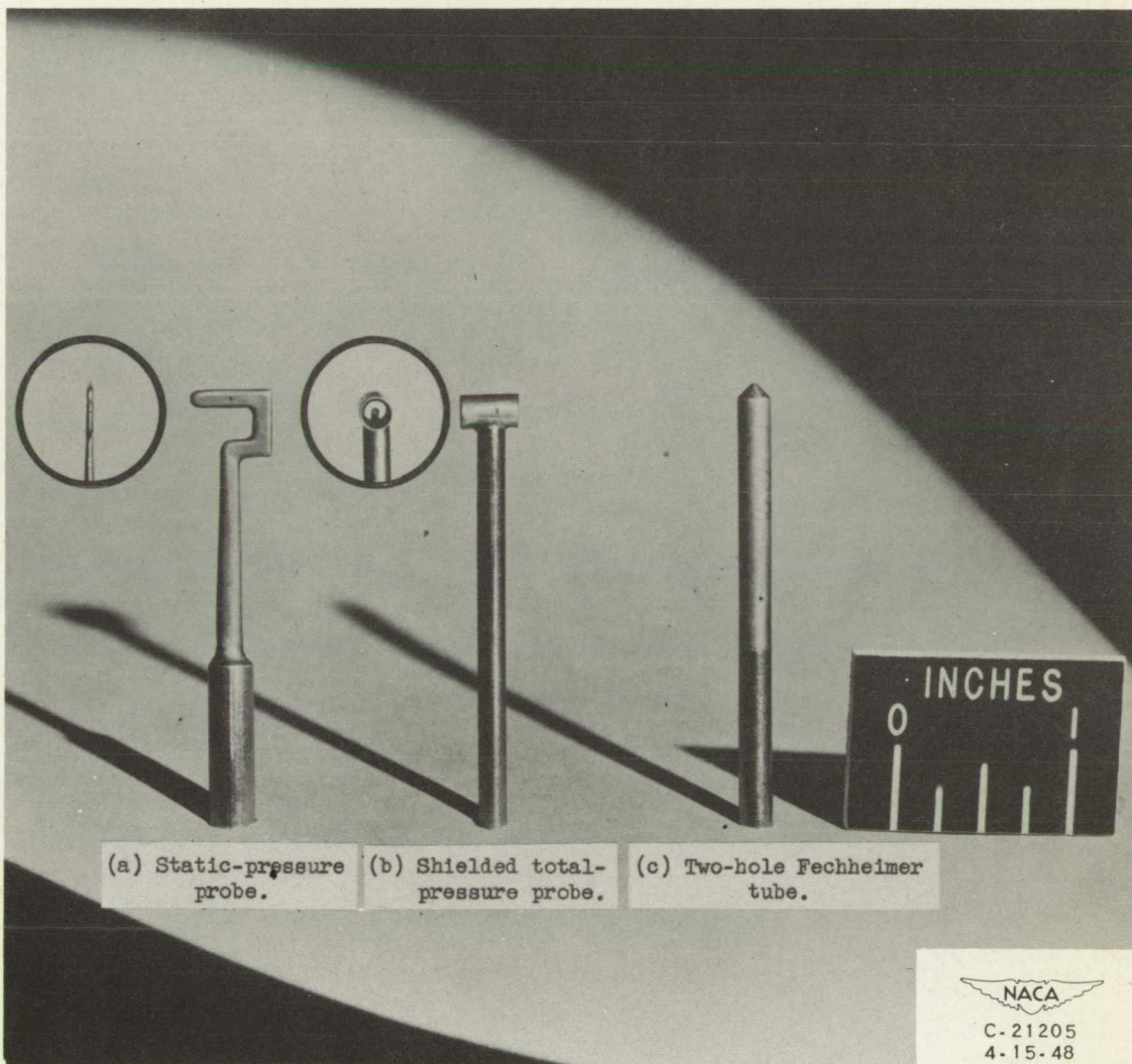
Figure 2. - Radial-survey instruments.

Page intentionally left blank

Page intentionally left blank
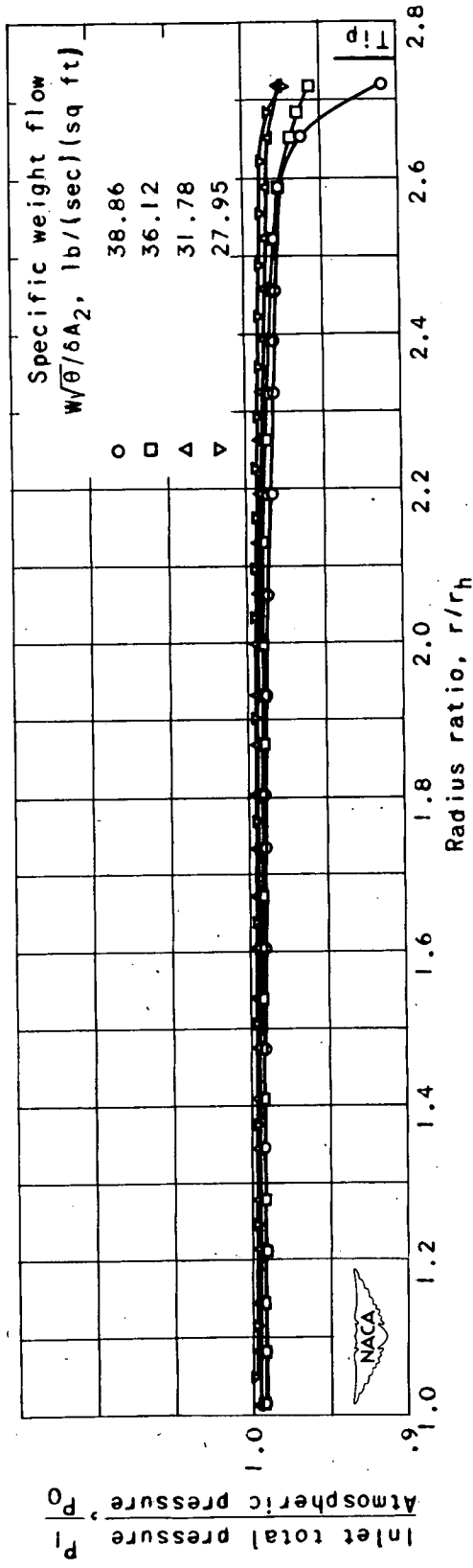
Figure 3. — Radial distribution of ratio of inlet total pressure to atmospheric pressure.
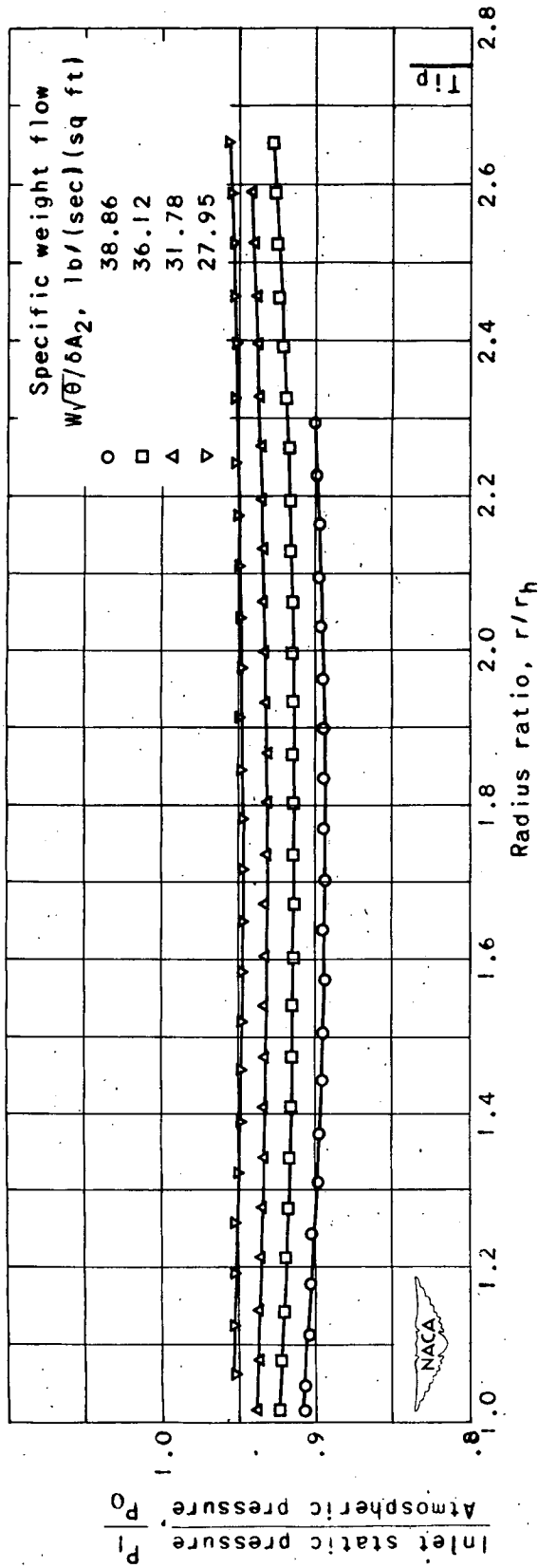
Figure 4. - Radial distribution of ratio of inlet static pressure to atmospheric pressure.
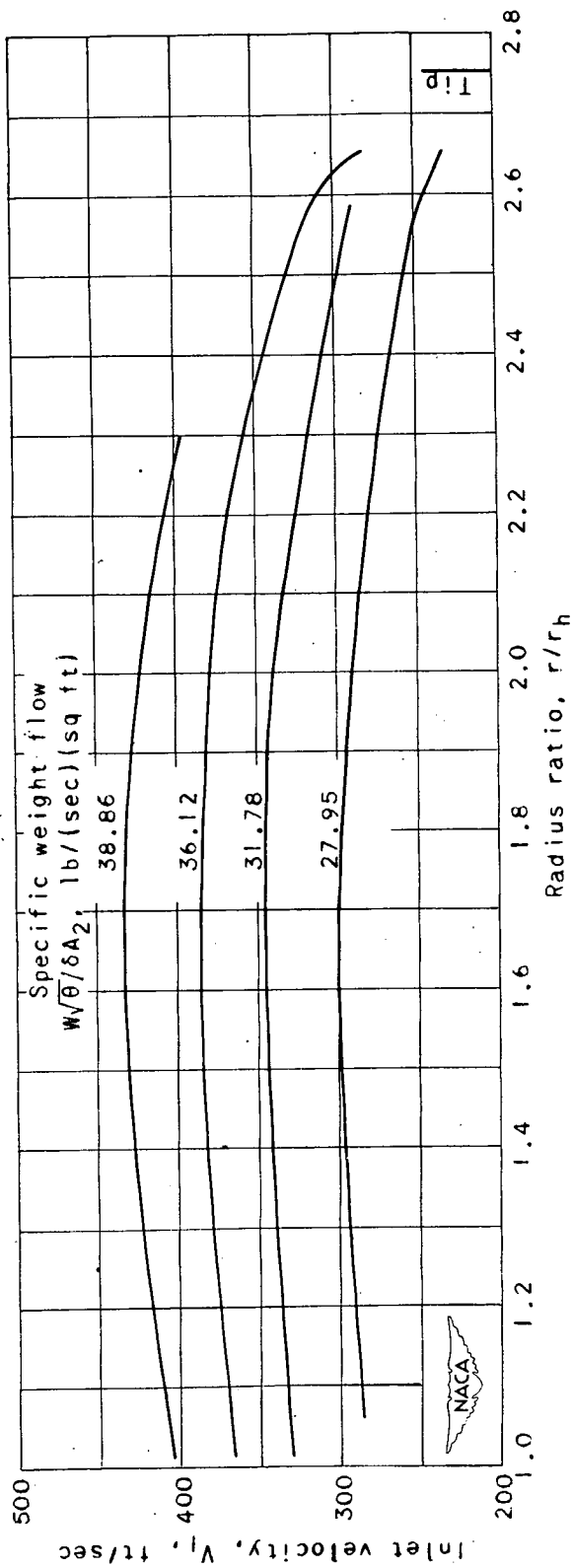
Figure 5. – Radial distribution of inlet velocity.
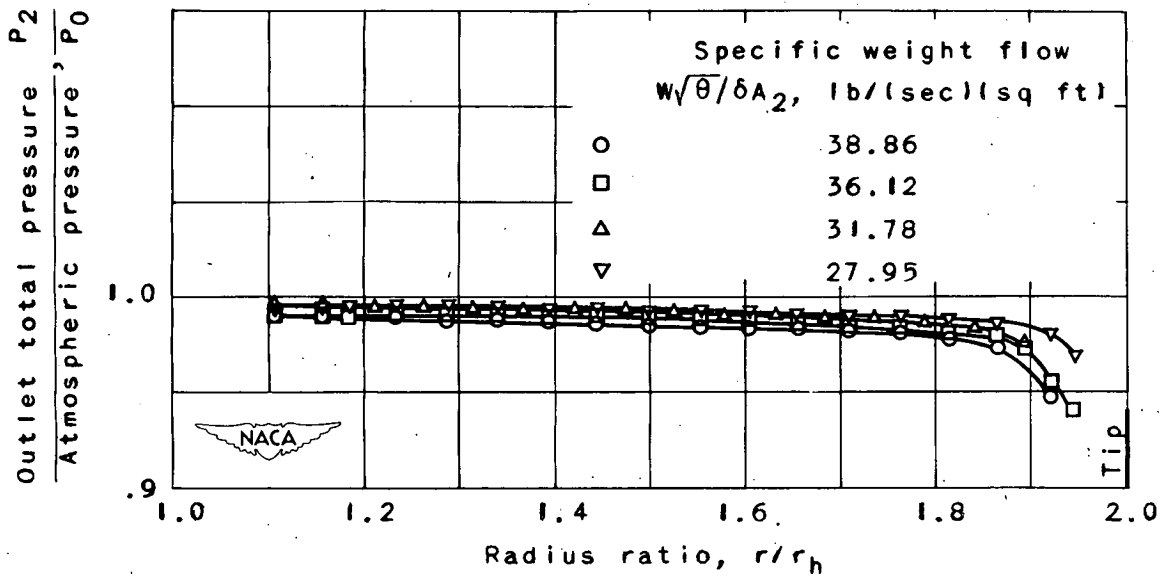
Figure 6. – Radial distribution of ratio of outlet
total pressure to atmospheric pressure.
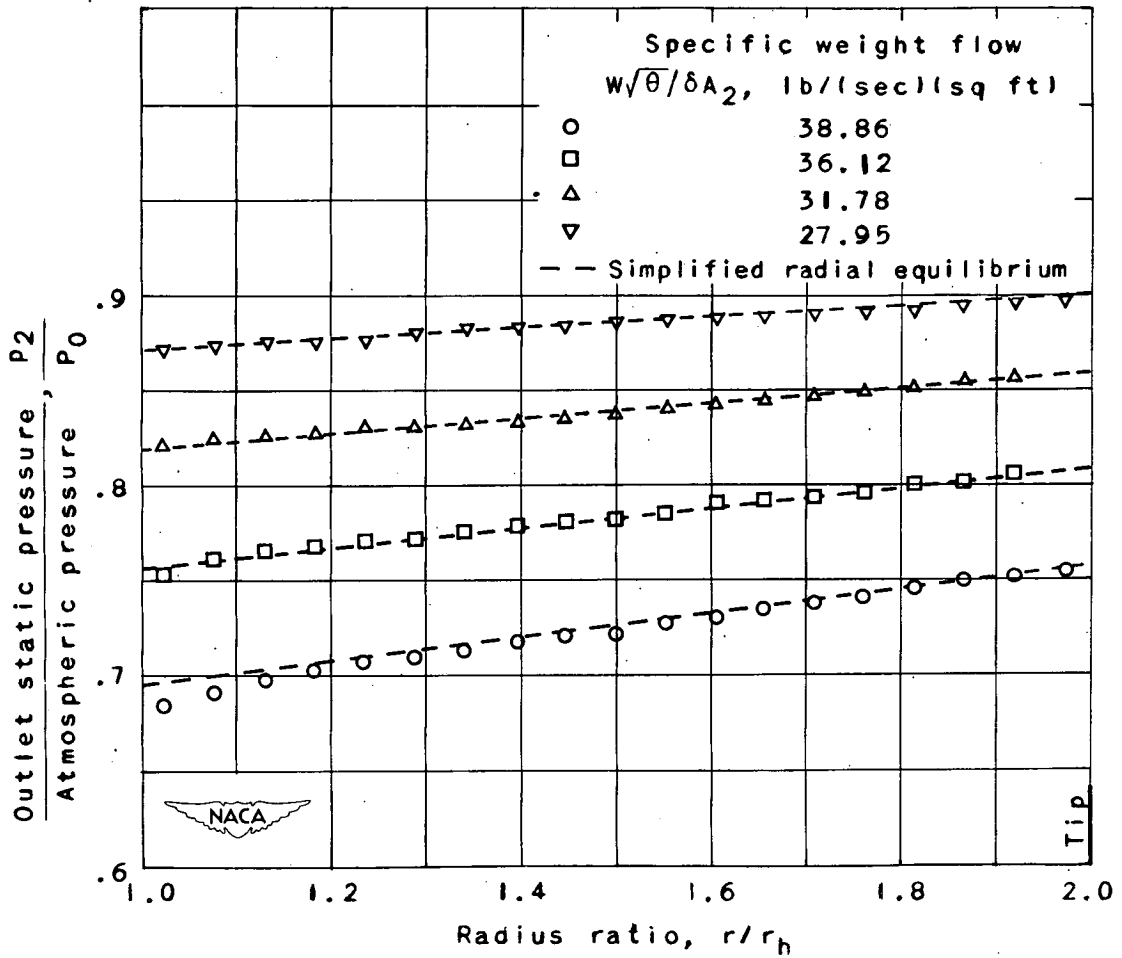
Figure 7. – Radial distribution of ratio of outlet static pressure to atmospheric pressure.
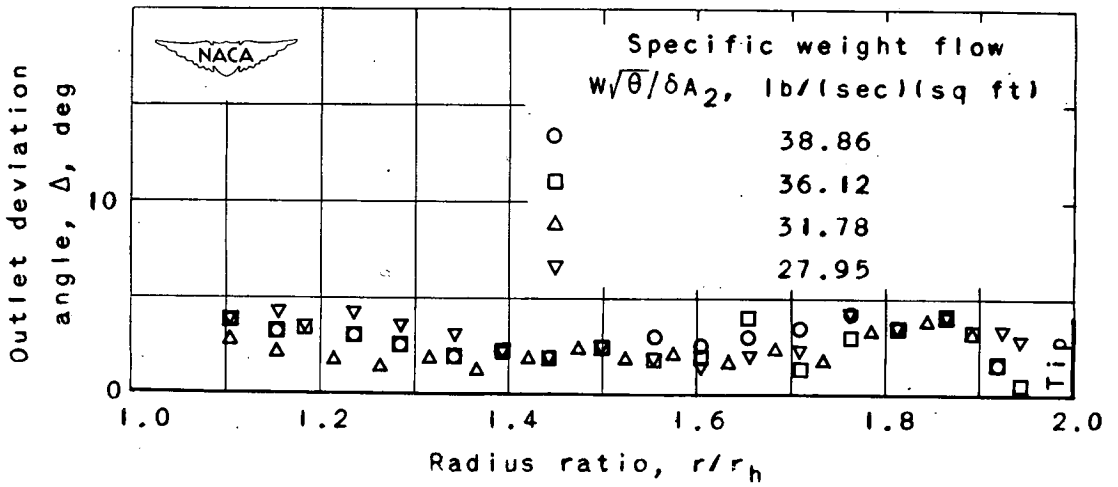
Figure 8. — Radial distribution of outlet deviation
angle.
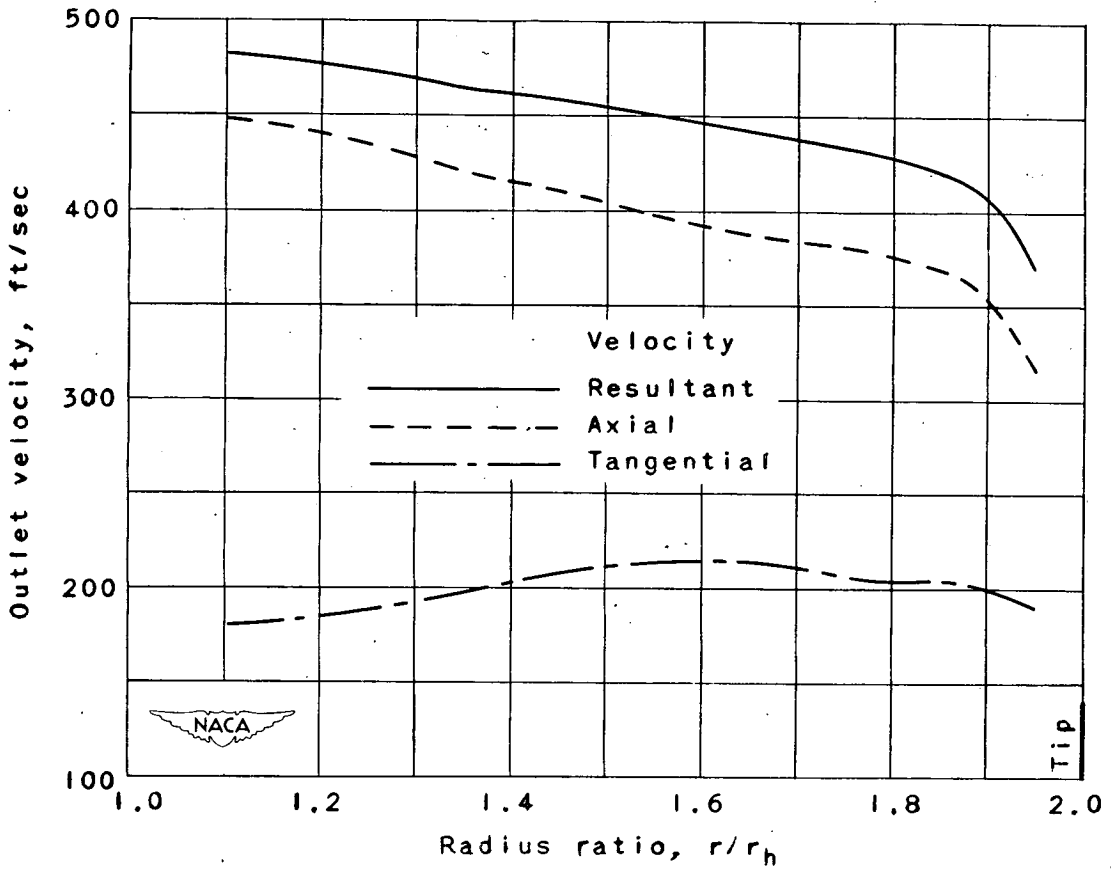
(a) Specific weight flow $W\sqrt{\theta}/\delta A_2$, 27.95 pounds per second per square foot.

Figure 9. - Radial distribution of outlet velocity.
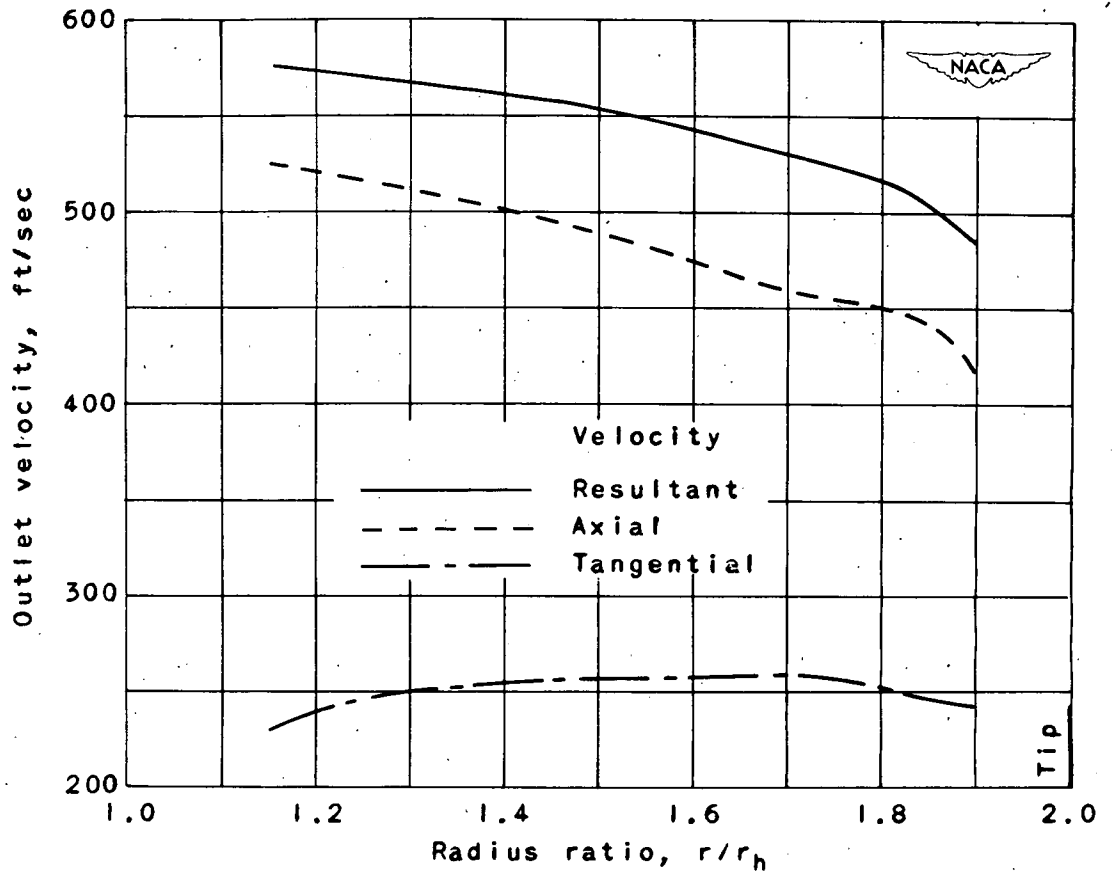
(b) Specific weight flow $W\sqrt{\theta}/\delta A_2$, 31.78 pounds per second per square foot.

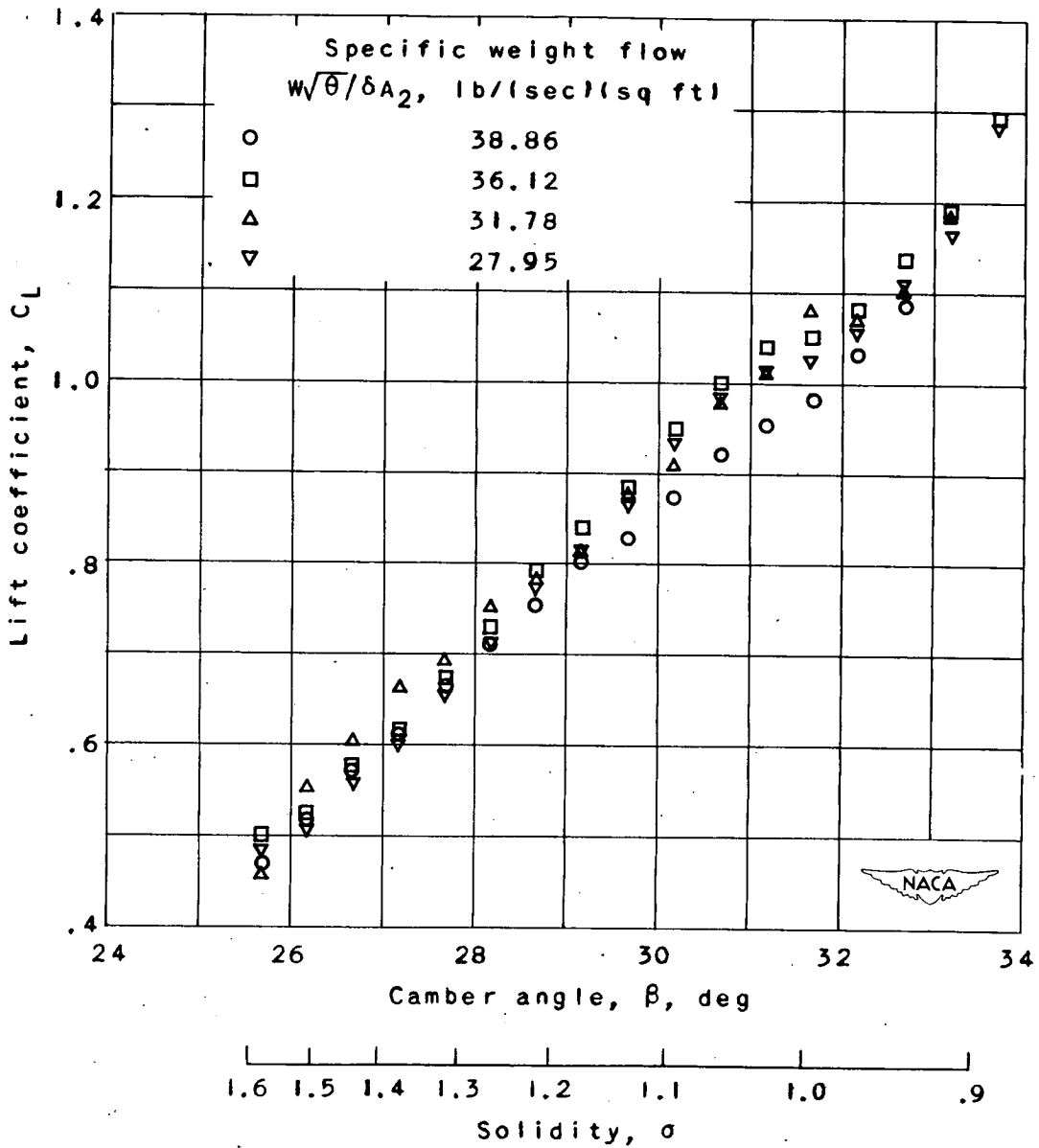Figure 9. – Continued. Radial distribution of outlet velocity.
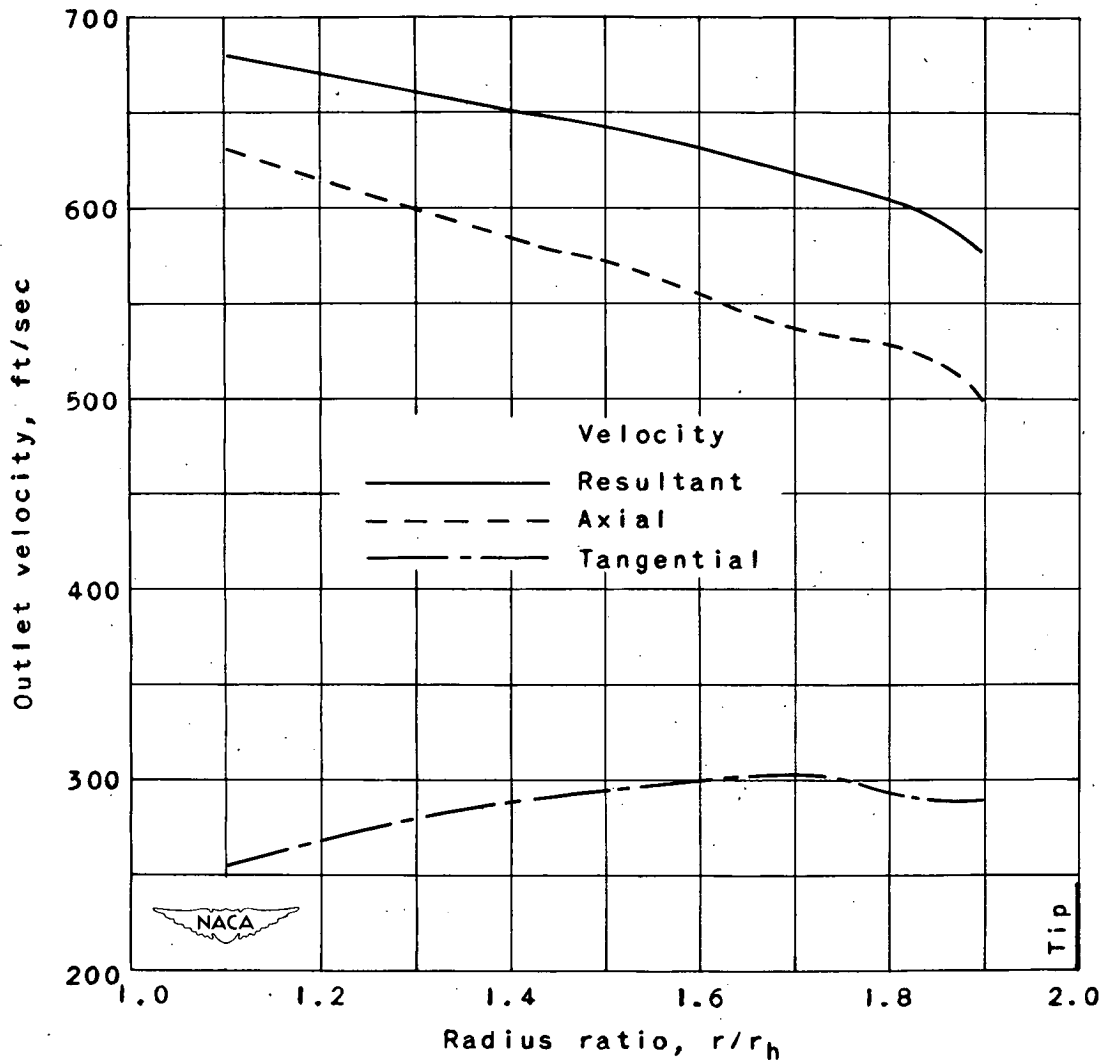
(c)   Specific weight flow $W\sqrt{\theta}/\delta A_2$, 36.12 pounds per second per square foot.

Figure 9.   - Continued.   Radial distribution of outlet velocity.
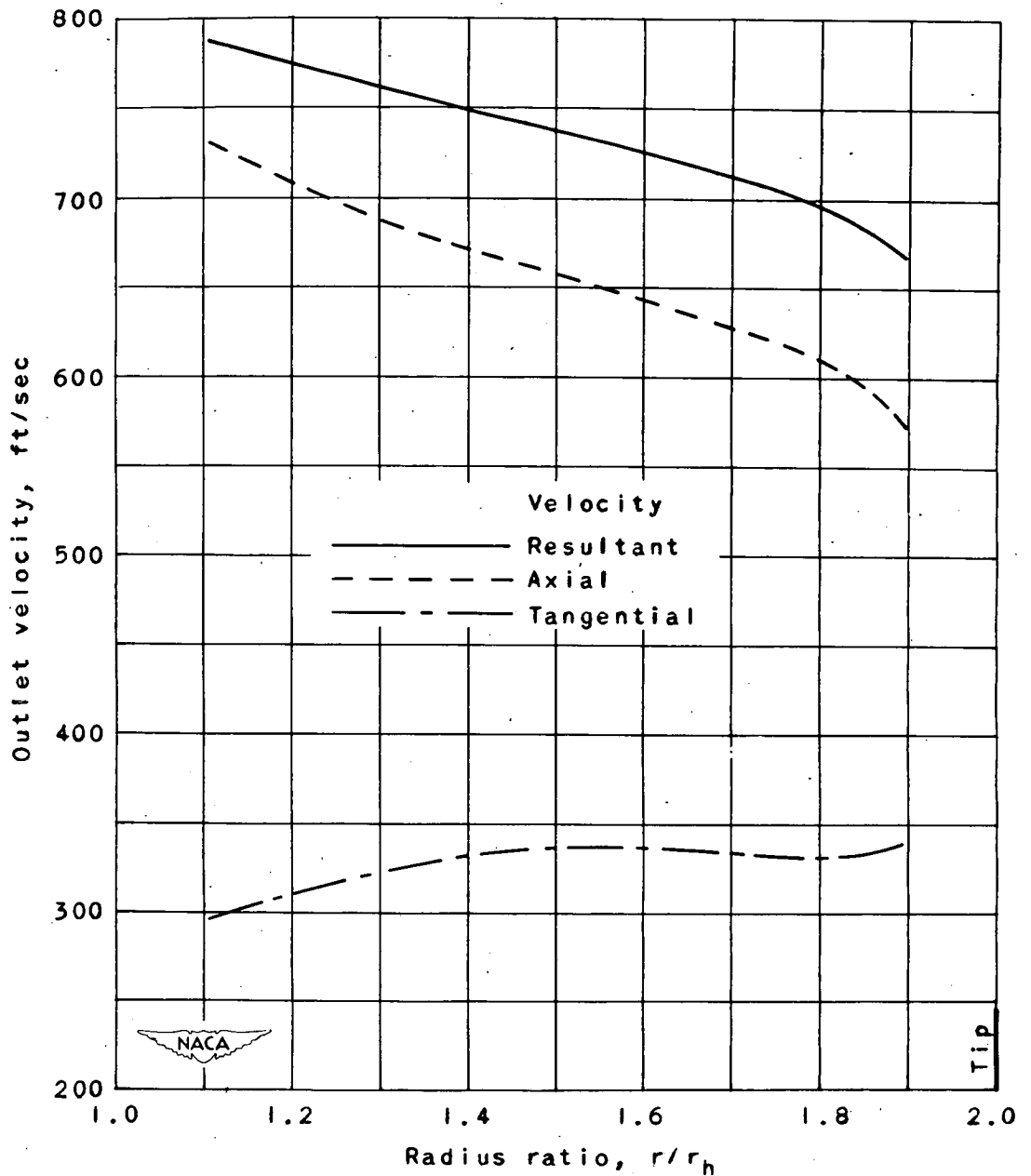
(d) Specific weight flow $W\sqrt{\theta}/\delta A_2$, 38.86 pounds per
second per square foot.

Figure 9. — Concluded. Radial distribution of
outlet velocity.

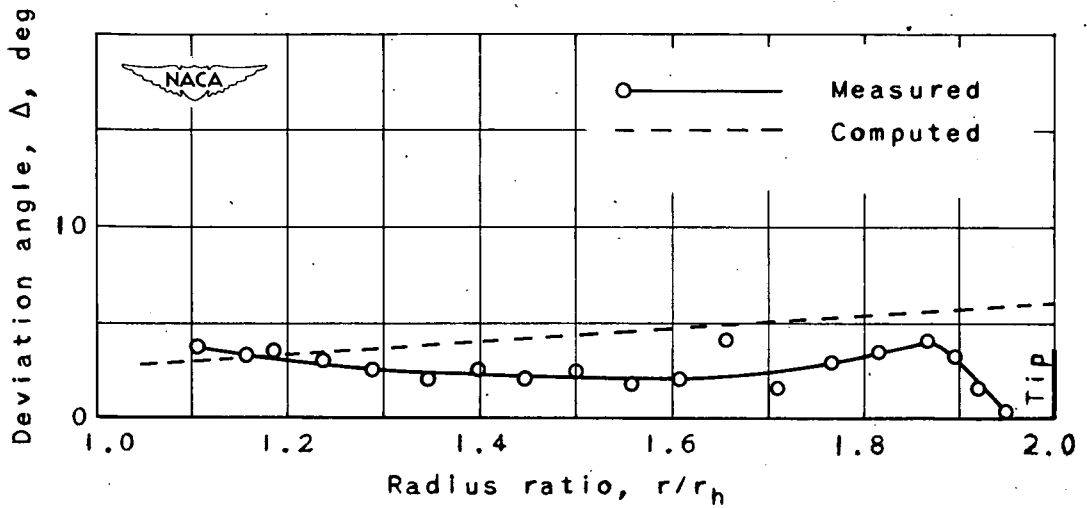Figure 10. – Variation of lift coefficient with camber
angle and solidity.

Figure II. - Comparison of measured deviation angles
with angles computed by rule based on Constant's work
(reference 2) for specific weight flow of 36.12
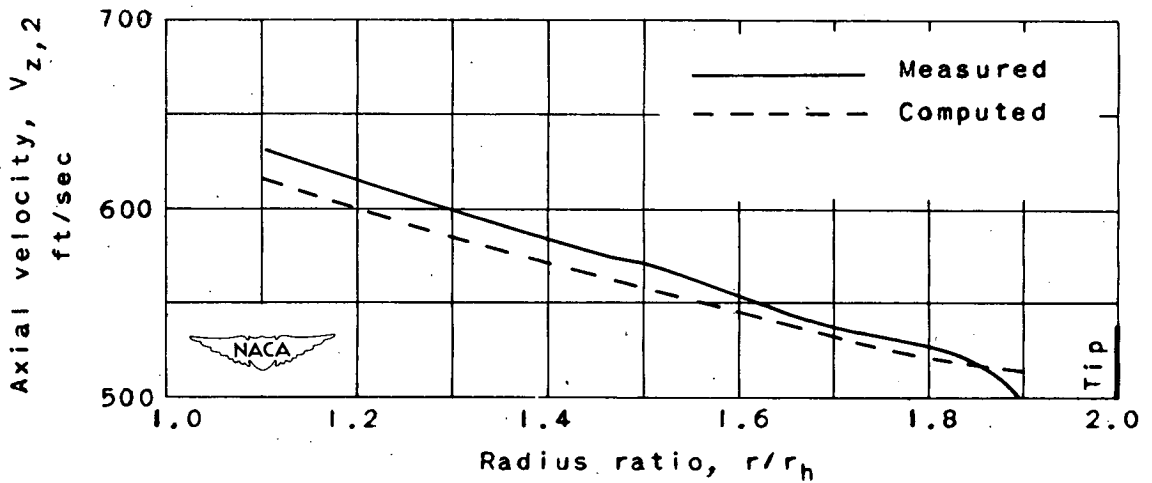pounds per second per square foot.

Figure 12. — Comparison of measured and computed
  axial velocities of outlet measuring station at
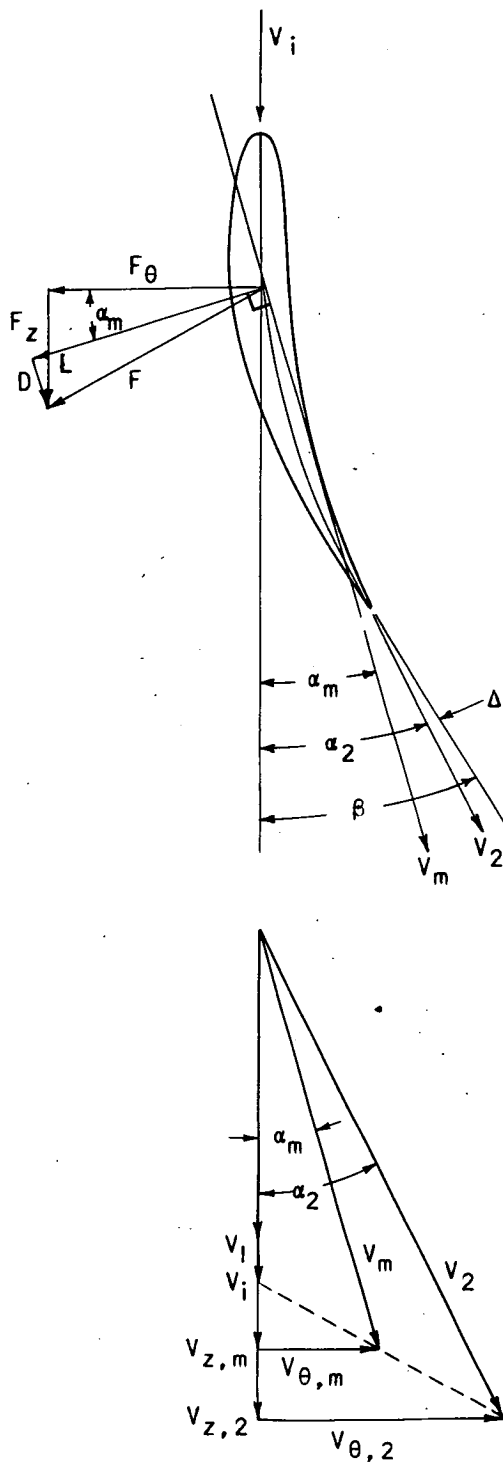 specific weight flow of 36.12 pounds per second
  per square foot.

Figure 13. – Vector diagrams of forces on blade
element and velocities through guide vanes.